Periodico di Mineralogia (2015), 84, 2, 373-388 DOI: 10.2451/2015PM0019

PERIODICO di MINERALOGIA
established in 1930

An International Journal of
MINERALOGY, CRYSTALLOGRAPHY, GEOCHEMISTRY,
ORE DEPOSITS, PETROLOGY, VOLCANOLOGY
and applied topics on Environment, Archaeometry and Cultural Heritage

Spectroscopic and nanoscale characterization of blue-coloured smithsonite ($ZnCO_3$) from Lavrion historical mines (Greece)

Michail Samouhos[1,*], Janez Zavašnik[2], Alexander Rečnik[2],
Athanasios Godelitsas[3], Elias Chatzitheodoridis[1] and Yiannis Sanakis[4]

[1] School of Mining and Metallurgical Engineering, National Technical University of Athens
157 80 Zographou, Athens, Greece
[2] Department for Nanostructured Materials, "Jožef Stefan" Institute, Jamova 39, 1000 Ljubljana, Slovenia
[3] Faculty of Geology & Geoenvironment, University of Athens,
Panepistimioupoli Zographou, 15784 Athens, Greece
[4] Institute of Nanoscience and Nanotechnology, NCSR "Demokritos", 15310 Ag. Paraskevi, Attica, Greece
[*] Corresponding authors: *msamouhos@metal.ntua.gr*

Abstract

Spectroscopic and microscopic (particularly HRTEM) techniques were used to investigate the origin of the colour of natural blue Zn-carbonate (smithsonite). Blue smithsonite is rich in copper, but substitution of zinc cations by copper cations, as proposed in the past for the origin of the colour, is questionable considering the absence of anhydrous divalent copper carbonates in nature. In this work, optical microscopy, SEM-EDS, XRD and laser micro-Raman could not resolve distinct phases either than Zn-carbonate, while NIR spectra excluded known chromophore Cu-hydroxycarbonate minerals. HRTEM studies however could clearly resolve nano-sized (3-7 nm) Cu-rich inclusions (specifically Si/Ca/Cu/As-rich inclusions of at least one phase), which are organised in bands with no topotaxial relation to bulk smithsonite. Electron-beam sensitivity of the samples, even at low electron current densities, did not allow the exact identification of the inclusions. However, it can be safely suggested, for the first time in the literature, that they are the cause of the blue colour in smithsonite.

Key words: Smithsonite; Zinc; Copper; Near Infrared Spectroscopy; Laser micro-Raman Spectroscopy; High-Resolution Transmission Electron Microscopy; Electron Paramagnetic Resonance; Nanophase.

Introduction

Colour in minerals and the role of nano-mineralogy

Colour is one of the properties that make minerals attractive, a property especially interesting for gemstones. It is also one of the basic diagnostic properties in their identification, although not exclusive. Colour is perceived by the human eye, and it is sensed by its light receptors when they interact with the different wavelengths of the visible spectrum. Mechanisms that cause colouration of minerals are summarised by Nassau (1978). For example, physical optic effects that can cause colouration and are based on the micro and nanoscale heterogeneities or periodicity in the structure of the bulk material include dispersion, interference, scattering, and diffraction (i.e., periodically deposited micro-particles of colloidal silica in opals induces colour due to iridescence phenomenon). Electronic transitions on metal impurities and on colour centres are another important mechanism to induce colour on minerals, and is explained by crystal field theory. Electronic transitions are a result of the presence of transition metals, rare earth elements, and other ions, which have incomplete electron shells, i.e., an incomplete set of 3d electrons either in the chemical formula of the mineral (idiochromatic), or as an impurity in its crystal lattice (allochromatic) (Nassau, 1978). Colour centres are created by the misplacement of an ion (and an unpaired electron takes its vacancy) or by the displacement of an electron due to natural or artificial radiation. An example of local colouration due to colour centres in minerals is when they host inclusions of other minerals that are rich in radioactive elements. Charge transfer causes colouration when the energy required for the transition of an outer shell electron between two charged ions (for example between Fe^{2+} and Fe^{3+}) is equivalent to energy within the visible spectrum (Nassau, 1978). Finally, band theory can explain mineral colouration when the absorbed white light has sufficient quantum energy for the transition of bonding electrons from the valence band to the conduction band. This mechanism takes place in case of minerals that behave as conductors, semiconductors, or contain impurities of dopant ions. Moreover, elements like boron are likely responsible for phosphorescence emissions related to the colour of distinct minerals such as diamonds (Gaillou et al., 2012).

It is now well known that mineral phase impurities that are the cause of colour in a variety of minerals are actually the result of nanoscale inclusions (i.e., mineral nanoparticles and nanominerals). 'Mineral nanoparticles' are actually common minerals that also occur in nanoscale sizes, whereas 'nanominerals' are specific phases which exist only in nanoscale, without equivalent crystals in larger scales (Waychunas, 2001; Udubasa et al., 2007; Hochella et al., 2008; Wauchunas and Zhang, 2008; Plathe et al., 2010). Inclusions of mineral nanoparticles (nanoinclusions) are important for the colour of minerals such as in quartz, where dumortierite $[Al_7BO_3(SiO_4)_3O_3]$ nano-fibers give the pink colour to crystals of quartz (Applin and Hicks, 1987; Goreva et al., 2001; Ma et al., 2002; Kibar et al., 2007). Despite some specific examples, the role of nanominerals in the colour of their host minerals has not been extensively investigated. In this case, in terms of chemical composition and structure the nanominerals can be new minerals, such as barioperovskite ($BaTiO_3$) that occurs as nanocrystals into benitoite (Ma and Rossman, 2008).

All of the above investigations suggest that the main way to study the origin of colour in minerals, particularly when they contain mineral nanoparticles and/or nanominerals is the combination of spectroscopic and microscopic techniques. In this work we used a set of analytical techniques to investigate the origin of the blue-coloured smithosnite

from Lavrion historical mines (Greece). The analytical instruments include High-Resolution Transmission Electron Microscopy (HR-TEM), Near Infrared spectroscopy (NIR), micro-Raman spectroscopy, Electron microscopy and X-Ray microanalysis (SEM/EDS). The HR-TEM technique has been proven the right tool which allows secure identification of nanominerals hosted in the matrix of other minerals.

Coloured smithsonites

Smithsonite is the naturally occurring single anhydrous zinc carbonate ($ZnCO_3$). It belongs to the calcite group of carbonate minerals conforming to the formula ACO_3, where A represents a large variety of cations such as Ca, Mg, Mn, Fe, Co, Ni, Zn, and Cd. Smithsonite crystallizes in the hexagonal-rhombohedral space group $R\bar{3}c$ (Reeder, 1983). Deposits of smithsonite are formed by the weathering of zinc-rich mixed sulphide ore bodies (supergene process). The main process is pyrite oxidation, which causes the production of sulphuric acid that further leaches sphalerite. Zinc dissolved in groundwater is transported through carbonate rocks and precipitates in the form of $ZnCO_3$ when the alkalinity of water increases (Hitzman et al., 2003; Skarpelis and Argyraki, 2008). Natural smithsonite is typically rich in metal cations (Ca, Mg, Fe, Pb, Zn, and Cu), which originate from either the primary sulphide ore or the body or the parent rock, leached by groundwater. It is generally accepted that these metal cations cause the colouration of smithsonite. Samples of smithsonite from several mines around the world have been examined demonstrating the existence of two causes of colouration; (a) due to chromophore mineral impurities, such as greenockite (CdS) and galena (PbS) inclusions contained in the yellow and green smithsonite, respectively (Katerinopoulos et al. 2005), or coronadite [$Pb(Mn^{+4}, Mn^{+2})_8O_{16}$] contained in milky smithsonite (Chen and Chang, 1975), and (b) due to zinc substitution by metallic divalent cations such as Mn^{+2} (Birch, 1986, Böettcher et al., 1993) and Ca^{+2} (Garcia-Guiunea et al., 2009). The substitution of Zn with Mn is a reliable explanation of the mechanism that causes colour to smithsonite since $ZnCO_3$-$MnCO_3$ solid solutions have been also synthesized in the laboratory at low temperatures (Böettcher, 1995).

In most of the cases, the cause of colourisation in smithsonites has been determined using spectroscopic techniques. Raman analyses of yellow, pink, and green smithsonites (Frost et al., 2007) show a shift of the main bands in comparison with the respective bands of clear smithsonite which can be attributed to a structural distortion on atomic level. Similar band sifts that appeared in the NIR spectra of coloured smithsonites from Namibia (Frost at al., 2006; Frost et al., 2008) reveal structural Ca^{+2}, Cu^{+2}, Cd^{+2}, and Fe^{+2} cation substitutions. Information concerning the presence of trace elements (Mg, Fe and Cu) in μm scale in smithsonites can be provided using the cathodoluminescence technique (Götte and Richter, 2004).

However, the cause of the blue colour in smithsonite has been poorly described. The absence of visible mineral inclusions using an SEM microscope in a number of blue Cu-rich smithsonite specimens from two renowned localities (Lavrion mines - Greece, Kelly mine - USA) led some researchers to the conclusion that substitution of Zn cations by Cu cations is possible (Frisch et al., 2002; Reddy et al., 2004; Katerinopoulos et al., 2005). In the study of Reddy et al., the presence of Cu^{+2} ions has been indeed determined using EPR technique, however, these results are not accompanied with microscopic data in order the absence of an included, in smithsonite, copper mineral be excluded. The absence of anhydrous divalent copper carbonate in nature, which could act as end-member in a potential $ZnCO_3$-$CuCO_3$ solid solution, support the idea that a possible substitution of Zn^{+2} ions by Cu^{+2} ions must be

further investigated and reconsidered.

We revisited this problem, with regard to the natural blue Zn-carbonate (smithsonite) that contains copper, in order to investigate it with additional spectroscopic and especially high-resolution microscopic techniques for acquiring structural information on the nanoscale level. We intended to clarify whether copper cations can replace zinc cations in the carbonate structure, or if zinc and copper form distinct chromophore phases. This is mainly due to the fact that anhydrous divalent copper carbonates, that could form potential solid solutions with anhydrous zinc carbonates (smithsonite), are not principally found to occur in natural environments. The studied sample originates from Lavrion historical mines (Attica, Greece).

Experimental procedures and conditions

The selected blue smithsonite from Lavrion mines (Attica, Greece) was obtained from the collection of the Mineralogical Museum of the National Technical University of Athens (NTUA). It has been most probably collected from underground works during ‘50s or ‘60s. A homogeneous bulk blue smithsonite fragment, with a mass of approximately 100 g, was extracted from the initial sample illustrated in Figure 1.

The bulk XRD (powder-XRD) characterization was performed using a Bruker D8 Focus diffractometer. Bulk chemical analyses were carried out by Atomic Absorption Spectroscopy (AAS) using a Perkin Elmer 2100 instrument. Bulk NIR spectra were obtained with a TerraSpec spectrometer.

Several thin-polished sections of the mineral were examined with an optical microscope. Chemical microscale analyses were performed by means of a Zeiss (LEO 1530 Gemini) Scanning Electron Microscope (SEM) equipped with an Oxford EDS and Cathodoluminescence system. The Laser micro-Raman spectra were obtained on thin-polished sections with a Renishaw Ramascope RM1000 equipped with a HeNe laser at 632.8 nm.

High-Resolution Transmission Electron Microscopy (HRTEM) studies were performed using a 200 kV Field-Emission microscope (JEM-2010F, JEOL Inc.) equipped with a slow-scan CCD camera (ORIUS SC1000A, Gatan Inc.) and electron energy dispersive spectrometer (EDS) using Si (Li) X-ray detector (Oxford Instruments Link ISIS 300, Oxford Instruments PLC). The specimen was cut perpendicular to the longer axis of the columnar smithsonite grains (Well Precision Diamond Wire Saw 3242) and mounted in a 3 mm support ring. The specimen was then thinned to 90 μm and dimpled down to 20 μm at the disc centre (Gatan Dimple grinder model 656). After grinding, the sample was ion milled (Bal-Tec Rapid etching system RES 010) by 4 keV Ar^+ ions to achieve electron transparency. In order to improve its electron conductivity the specimen was coated by 3 nm of amorphous carbon (PECS 682, Gatan Inc.).

Figure 1. Blue Cu-bearing smithsonite sample from Lavrion historical mines (courtesy of the Mineralogy and Geology Museum of the NTUA, Greece).

X-band EPR measurements were carried out on an upgraded Bruker ER-200D spectrometer equipped with an Anritsu MF76A frequency counter, and a Bruker 035M NMR Gaussmeter. The spectra were simulated by using the SpinCount package (Prof. M.P. Hendrich, Carnegie Mellon University).

Result and Discussion

Bulk characterization (powder-XRD, AAS chemical analyses and NIR spectroscopy)

The powder XRD pattern of the Lavrion blue smithsonite is presented in Figure 2. All peaks (with major d spacings at 3.55, 2.75, 2.33, 2.11 and 1.71Å) correspond to smithsonite ($ZnCO_3$) PDF database reference number ICDD-00-008-0449. No other mineral phase was detected in the pattern with this characterization technique. The bulk (AAS) chemical analyses of the sample reported in Table 1 indicate, apart from Zn, the presence of noticeable amounts of Cu, Ca, Cd and Mg cations, while minor amounts of Mn, Pb and Fe cations were also detected.

The bulk near-NIR absorption spectrum of the studied blue smithsonite in comparison with NIR spectra of Cu-hydroxycarbonates, namely azurite [$Cu_3(CO_3)_2$ $(OH)_2$] and malachite [Cu_2CO_3 $(OH)_2$] exhibiting characteristic colours, is presented in Figure 3. There is no peak matching and therefore the existence of the above chromophore minerals should be excluded.

Microscale characterization (optical microscopy, SEM-EDS and micro-Raman)

Thin-polished sections of blue smithsonite were examined under an optical microscope (Figure 4) showing banding of dark blue and light blue colours, over its well-expressed rhombohedral cleavage. The electron microprobe (SEM-EDS) analyses (Table 2) proved the presence of trace metal impurities in the studied natural $ZnCO_3$, particularly Cu, Ca, Mg, Cd, Mn and Fe. Moreover, it was proved

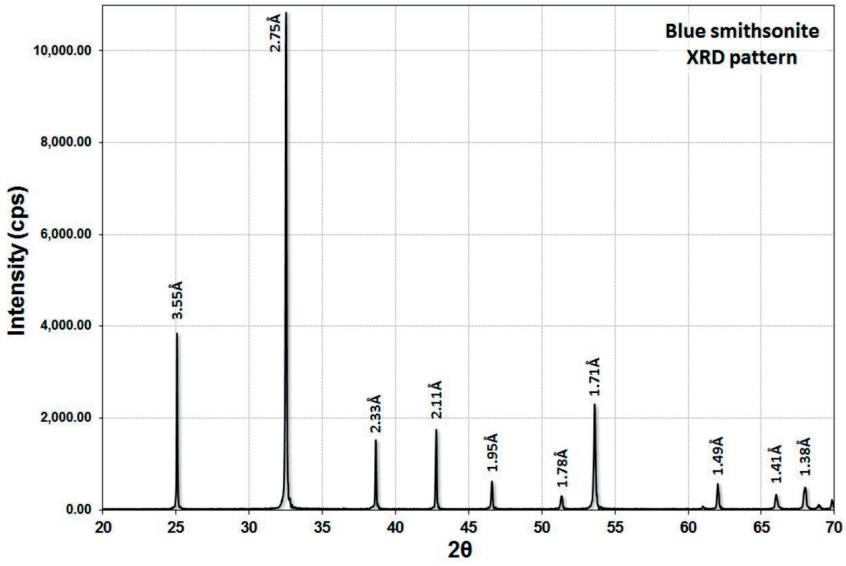

Figure 2. Powder-XRD pattern of the studied blue smithsonite.

Table 1. Bulk chemical analysis (AAS) of the blue smithsonite sample.

	wt%	wt% (normalized)
ZnO	64.23 ± 0.64	95.74
CuO	0.88 ± 0.01	1.31
CaO	1.25 ± 0.01	1.86
MgO	0.05 ± $5 \cdot 10^{-4}$	0.07
CdO	0.57 ± 0.01	0.85
MnO	0.04 ± $5 \cdot 10^{-4}$	0.06
FeO	0.07 ± $5 \cdot 10^{-4}$	0.10

that higher Cu concentration occurs in areas of dark blue colours observed under optical microscope (Figure 5). The dark blue coloured areas were logged in optical microscope in order to be further investigated with scanning electron microscopy. A triangular plot concerning selected trace elements in the studied smithsonite and various smithsonites (Götte and Richter, 2004) is presented in Figure 6. As can be seen in the plot, the studied sample presents a relatively homogeneous distribution concerning the presence of copper cations. The point analyses (SEM-EDS) analyses show stoichiometric composition whereas the bulk analyses (AAS) are not stoichiometric, suggesting the presence of other phases in the analysed bulk carbonate material that we analysed. It should be noted that Ca, Cd and Mg cations may be incorporated in the Zn-carbonate forming a variety of solid solutions (due to similarities of smithsonite, calcite, otavite and magnesite structures) while the involvement of Cu cations, as already mentioned, is rather doubtful.

The Raman spectrum of blue smithsonite at 298 K in the 180 to 1800 cm^{-1} region is shown in Figure 7. For comparison, the Raman

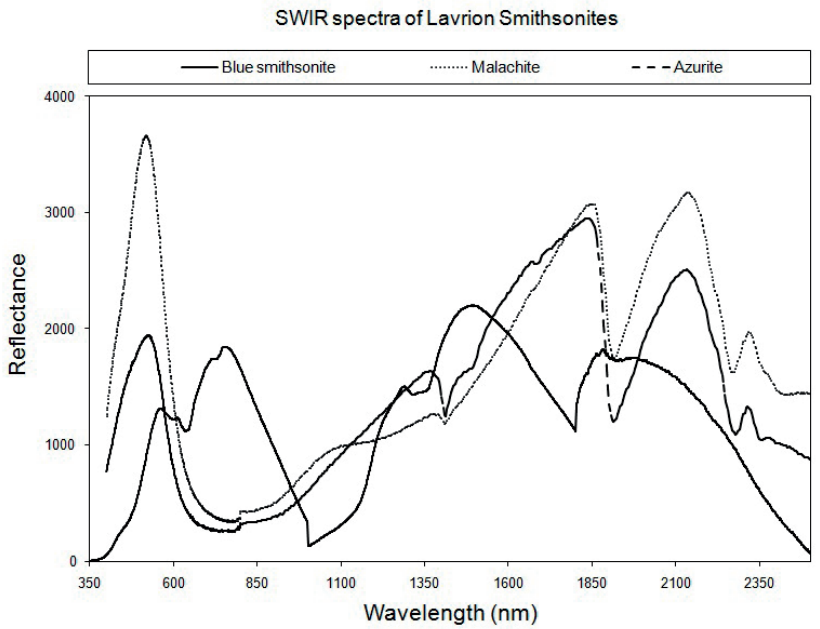

Figure 3. NIR bulk spectra of blue smithsonite sample in comparison with the respective spectra of azurite and malachite.

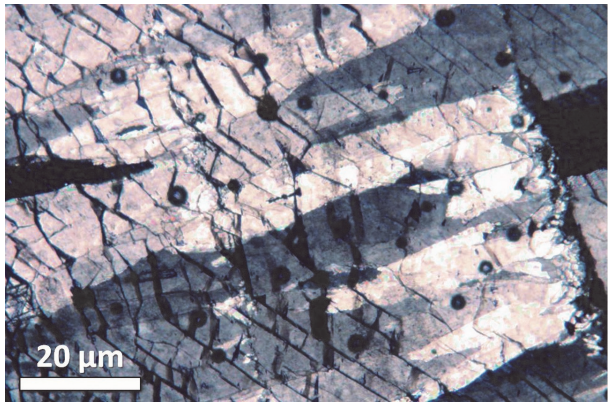

Figure 4. Optical microscope image (thin-polished section) of the blue smithsonite. Bluish banding is observed together with its cleavage.

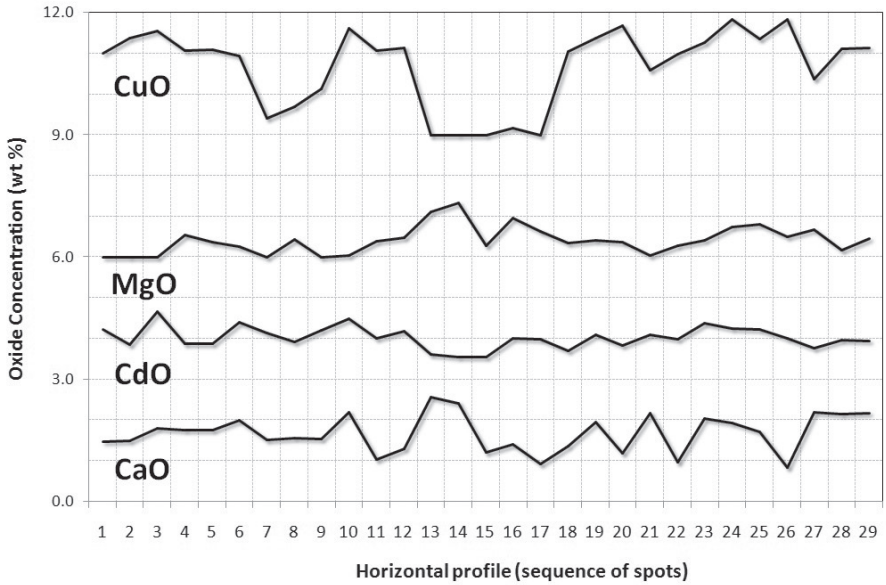

Figure 5. Electron microprobe (SEM-EDS) linescans showing chemical banding of the trace elements in blue smithsonite. The lateral step of each spot analysis is 1 µm. High values of copper coincide with darker blue colour bands.

Table 2. Electron microprobe analyses of the blue smithsonite sample (wt% normalized). The relative error of the microprobe analyses was about 0.2%.

ZnO	CuO	CaO	MgO	CdO	MnO	FeO
98.51	0.00	1.23	0.30	0.55	0.00	0.00
98.08	0.97	1.65	0.00	0.00	0.00	0.00
97.74	0.00	0.95	0.64	0.99	0.23	0.00
97.61	0.96	1.64	0.00	0.00	0.00	0.00
97.49	1.38	1.13	0.00	0.00	0.00	0.00
97.02	1.37	1.12	0.48	0.00	0.00	0.00
96.80	0.17	1.42	0.97	1.02	0.00	0.00
96.66	0.42	1.52	0.00	1.14	0.00	0.00
96.50	1.56	1.09	0.00	0.00	0.00	0.00
96.39	0.69	1.58	0.45	0.93	0.16	0.06
96.18	0.00	2.59	1.13	0.63	0.00	0.00
96.13	2.06	1.38	0.35	0.71	0.00	0.00
96.08	1.14	1.56	0.01	1.21	0.00	0.01
96.04	1.55	1.09	0.00	0.00	0.00	0.00
96.02	0.00	3.16	0.00	0.00	0.00	0.00
95.55	1.38	1.56	0.00	0.00	0.00	0.00
95.40	2.08	1.05	0.40	1.02	0.00	0.00
95.33	0.07	2.42	1.34	0.55	0.00	0.00
95.27	2.02	1.48	0.00	1.23	0.00	0.00
95.25	2.39	1.50	0.00	0.86	0.00	0.00
95.10	1.99	0.99	0.28	1.00	0.00	0.23
94.99	1.59	2.18	0.05	1.10	0.10	0.00
94.99	2.84	0.89	0.50	1.01	0.00	0.00
94.92	1.37	2.20	0.69	0.18	0.32	0.00
94.89	2.09	1.77	0.55	0.89	0.00	0.00
94.88	2.70	1.21	0.38	0.85	0.36	0.02
94.82	2.09	1.77	0.37	0.89	0.00	0.00
94.47	2.12	2.15	0.19	0.97	0.00	0.00
94.46	2.14	2.18	0.47	0.95	0.00	0.00
94.38	1.95	2.00	0.26	1.41	0.00	0.00
94.37	2.14	1.31	0.49	1.19	0.17	0.00
94.35	1.81	2.40	0.00	0.00	0.00	0.00
94.32	2.40	1.97	0.42	1.12	0.18	0.13
93.97	2.55	1.80	0.00	1.68	0.00	0.00
93.90	1.80	2.39	0.00	0.00	0.00	0.00
93.54	2.36	1.73	0.81	1.24	0.22	0.11
93.34	2.62	2.20	0.04	1.49	0.10	0.00
92.91	2.84	1.94	0.74	1.26	0.10	0.15

spectrum of a white smithsonite is also given. Both spectra are identical, indicating that no other phases can be detected with this technique, which could be a possible cause of the blue colour. Compared to smithsonite spectra taken from the literature we observe common bands, such as the intense Raman band at 1093 cm^{-1}, which is caused by the v_1 symmetric stretching vibration of the carbonate group, and the weaker bands at 730 and 1408 cm^{-1}, which are caused by the v_4 out-plane bending mode and the v_3 anti-symmetric stretch of the CO_3^{2-} ion respectively (Frost et al., 2007; Hales & Frost, 2007). The bands at 195 and 304 cm^{-1} are crystal lattice bands and they are attributed to the ZnO symmetric stretching vibration and the OZnO bending modes respectively (Frost et al., 2007; Hales & Frost, 2007). We do not observe the 870 cm^{-1} v_2 in-plane bending mode of CO_3^{2-}, while we observe an additional band at 1735 cm^{-1}, which is also reported in the study of Frost et al. (2007).

The band positions of blue smithsonite Raman spectrum are in excellent agreement with the respective band positions of pure synthetic smithsonite. We compiled a graph (Figure 8) correlating the major Raman peak v_1 at 1093 cm^{-1} with the crystal ionic radius of each metallic cation of the monometallic carbonates (Shannon, 1976). A clear and

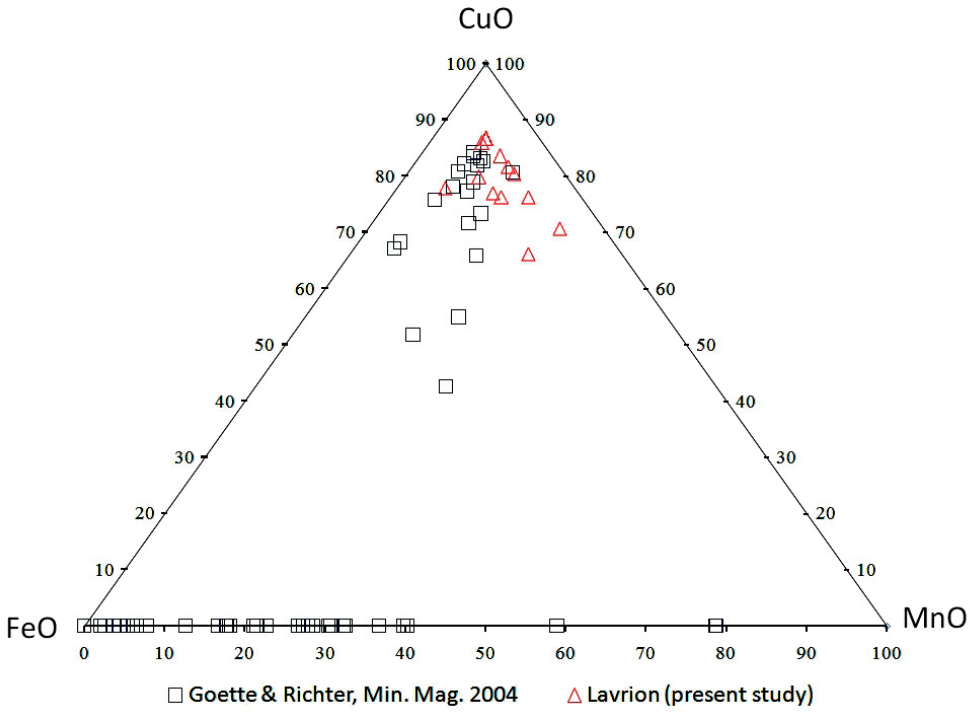

Figure 6. Triangular plot concerning Cu-Mn-Fe content (Wt%) of smithsonites (blue smithsonite of the present study: red triangles; various smithsonites from Götte & Richter, 2004: blue squares).

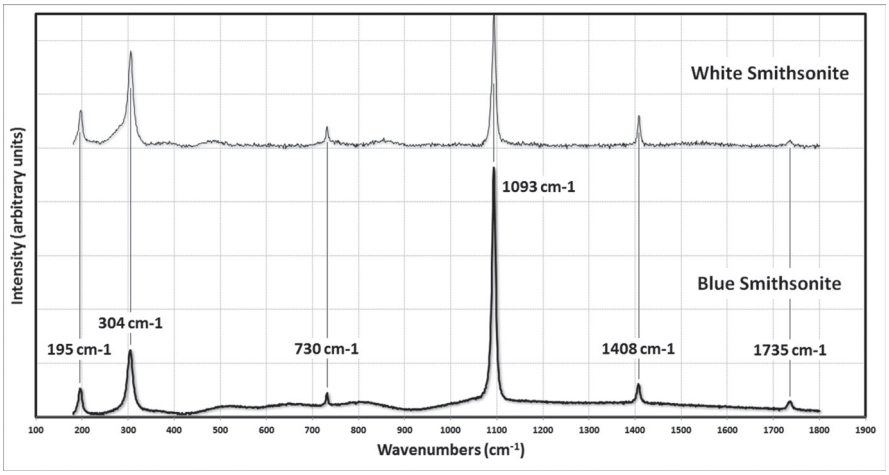

Figure 7. Representative Laser micro-Raman spectrum of blue smithsonite (thick line) compared to the spectrum of a white smithsonite (thin line).

systematic correlation is observed for the different cations as band shifting. For example, the Zn^{2+} ion of the $ZnCO_3$ lattice is possible to be substituted by Mg^{+2}, Mn^{+2} and Fe^{+2} ions and shifting along the correlation line is expected. Our blue smithsonite however does not show any band shifting or band widening, indicating the lack of significant substitution of Zn^{2+} ion by other metallic ions and the creation of a solid solution. Moreover, the concentration of the above-mentioned cations is extremely low in case of the investigated blue smithsonite and these cations do not constitute chromophores of blue colour.

Nanoscale characterization (HRTEM-EDS) and EPR spectroscopy

TEM Energy Dispersive Spactra (EDS) study was applied to detect nanoscale inclusions contained in smithsonite volume. The sample was cut out of the botryoidal bulk material with no visible inter-crystal faces. The columnar nature of the aggregate, however, is evident from fractured fragments of the specimen. Smithsonite crystals are densely populated with various types of inclusions, among which quartz grains are the most dominant. In addition, the crystals are disrupted by dislocations and domain boundaries. Figure 9a shows a bright field TEM image of smithsonite crystal tilted to its [010] orientation. Under high current densities, *i.e.*, HRTEM imaging conditions (Figure 9c), the specimen displays sensitivity to electron irradiation, visible as rapid local amorphisation of the specimen. Electron diffraction pattern (EDP) recorded over the fault-free crystalline area is shown in Figure 9b. The measured d-values correspond to those for $ZnCO_3$ (PDF #83-1765) and are consistent with powder-XRD data (Table 3).

The majority of the inclusions are concentrated in bands (zones) inside the smithsonite crystal (Figure 10). Larger oval-shaped inclusions belong to quartz (SiO_2) grains, which are very sensitive to electron irradiation and become amorphous even at low electron doses. Smaller inclusions measuring 3-7 nm in diameter are Cu-rich, as shown by TEM-EDS measurements. The inclusions are not crystallographically

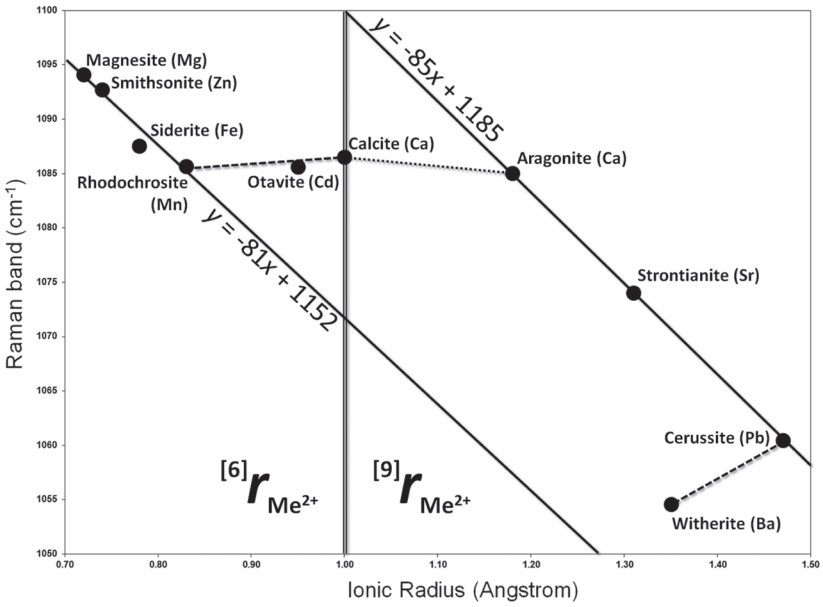

Figure 8. Correlation of the wavenumber of Raman main band of monometallic carbonates with the ionic radius (according to Shannon, 1976) of their cations. Points for each mineral are averages of measurements with standard deviations lower that the radius of the circle. Left from the vertical double line (at ionic radius equal to 1Å) are the carbonates with metallic ions of coordination 6 and to the right with coordination 9. Our blue smithsonite sample plots exactly at the point of smithsonite on the graph within error.

oriented in respect to the smithsonite lattice. Due to their small size the inclusions produce faint rings in the reciprocal space. To increase the contribution of nano-sized inclusions in cumulative EDP, the host crystal was tilted away from strong scattering conditions. The d-values (Table 4) of the diffraction rings (Figure 10b) do not overlap with the diffraction spots of smithsonite, indicating that they belong to a different phase. HRTEM image of the area with nano-sized Cu-rich inclusions is shown in Figure 10c. Any attempts of producing a small diameter probe for accurate EDS analysis of individual nano-sized particles that are embedded in the smithsonite matrix immediately results in severe amorphisation of the host crystal. Because the analysis of separate inclusions was not possible, several spectra were recorded over the larger areas with the inclusions, such as those shown in Figure 10b. The spectra consistently showed a significant increase in Si, Ca, Cu and As content. At different locations the ratio (Si, Ca) *vs.* (Cu, As) varied, implying that the inclusions belong possibly to two different phases. This also explains why the diffraction rings in the cumulative EDP could not be simply indexed to any known Cu compound. Thus we could demonstrate herein that a nanoscale Si-Ca-Cu-As phase, constituting in fact a novel nanophase, is occluded in the studied natural Cu-containing $ZnCO_3$. This nanophase may be responsible for the blue colour of this smithsonite from the historical Lavrion mines.

Electron Paramagnetic Resonance (EPR) spectroscopy has been used in order to investigate whether Cu ions are in the form of isolated Cu^{2+} cations (potentially substituting Zn^{2+} in the smithsonite matrix) or in some form

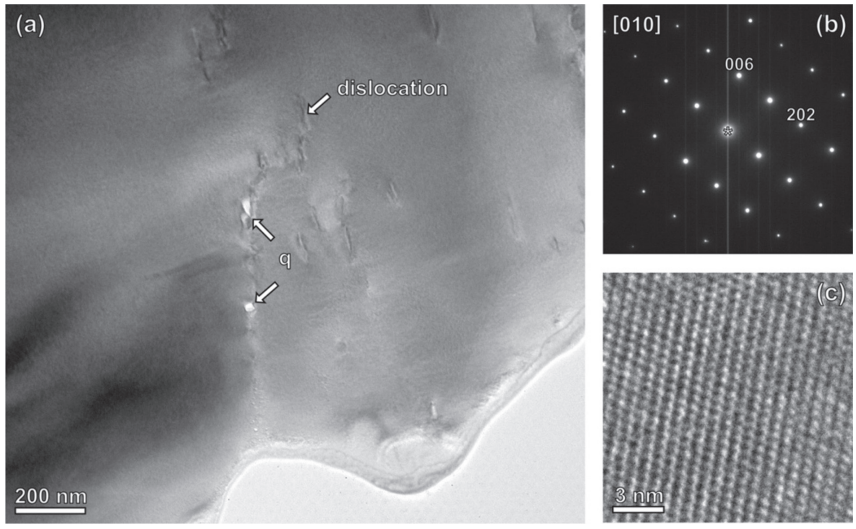

Figure 9. Bright-field TEM image of the blue smithsonite with dislocations and quartz (q) inclusions. (b) SAED pattern recorded over the inclusion-free area of the specimen, d-values are listed in Table 3. (c) Corresponding HRTEM image of smithsonite recorded along the crystallographic [010] axis.

of aggregates. The X-band EPR spectrum from a powdered sample recorded at room temperature is presented in Figure 11. The strongest feature in the spectrum is a set of six strong sharp lines accompanied by much weaker signals between them. This pattern is readily attributed to Mn^{2+}(S = 5/2) isolated ions in an octahedral environment. The spectra were simulated by the spin Hamiltonian (Abragam and Bleaney, 1970):

$$H = \mathrm{D}[S_z^2 - 2] + \mathrm{E}\,[S_x^2 - S_y^2] + \mathrm{I}\,A\,\mathrm{S} + \mathrm{g}\beta\,S\,\mathrm{H} \quad (1)$$

in which D and E are the axial and rhombic Zero Field Splitting parameters, respectively (Abragam and Bleaney, 1970). *A* represents the tensor of the hyperfine interaction between the

Table 3. Measured d-values from SAED and powder-XRD patterns for Lavrion blue smithsonite compared with standard d-values for $ZnCO_3$ (JCPDF #83-1765).

	D_1	D_2	D_3	D_4	D_5
$(hkl)_{smithsonite}$	(012)	(104)	(006)	(202)	(116)
PDF #08-0449 [Å]	3.551	2.747	2.504	1.945	1.704
measured TEM [Å]	3.56	2.71	2.50	1.92	1.72
measured XRD [Å]	3.55	2.75	2.33	1.95	1.71

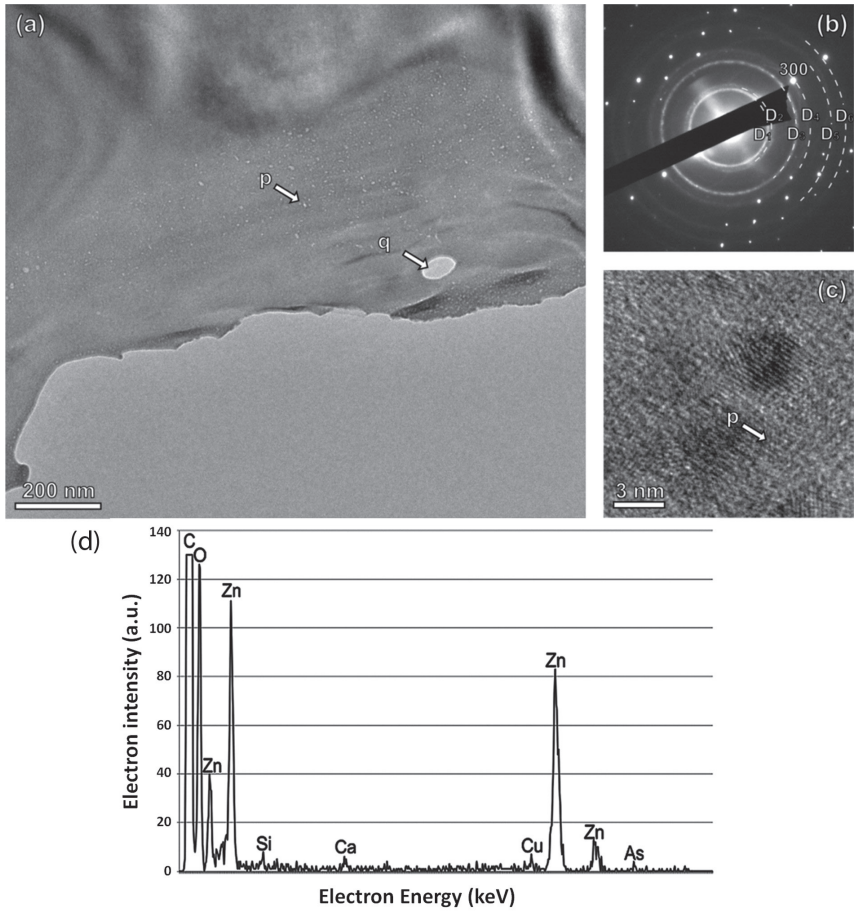

Figure 10. Bright-field TEM image of nano-sized Cu-rich inclusions (p) and larger xenomorphic grains belong to quartz (q) (a). SAED pattern recorded from this area shows diffraction rings with d-values specific for the Si-Ca-Cu-As nanophase (Table 4). The sample was tilted away from the zone axis to increase the contribution of the inclusions in the EDP (b). HRTEM image of Cu-rich inclusions (p) embedded in the smithsonite matrix (c). TEM-EDS spectrum indicating increased Si, Ca, Cu and As (d).

electronic (S = 5/2) and the nuclear spin (I = 5/2) of the ^{55}Mn nucleus. The spectra are reproduced with g = 2.0, |D|=0.007 cm^{-1}, E /D = 0, A = 257 MHz and including a Gaussian distribution in D with width σ_D = 0.005 cm^{-1}. Similar signals were observed in smithsonite samples (Reddy et al., 2004) and are attributed to Mn substituting Zn in $ZnCO_3$.

A closer examination of the spectrum indicates a broad weak signal in the 260 - 300 mT magnetic field range. This part of the spectrum has been magnified in the figure for the sake of clarity and could represent Cu^{2+} species. The lack of distinct hyperfine splitting in the spectrum indicates considerable spin-spin interactions which is inconsistent with isolated Cu^{2+} ions in $ZnCO_3$ matrix as it is clearly the case for the Mn^{2+} ions. Most probably the spectrum

Table 4. Measured d-values from SAED pattern for Si-Ca-Cu-As nanophase occluded in the blue Lavrion smithsonite

	D_1	D_2	D_3	D_4	D_5	D_6
measured TEM [Å]	2.78	2.45	1.59	1.35	1.02	0.92

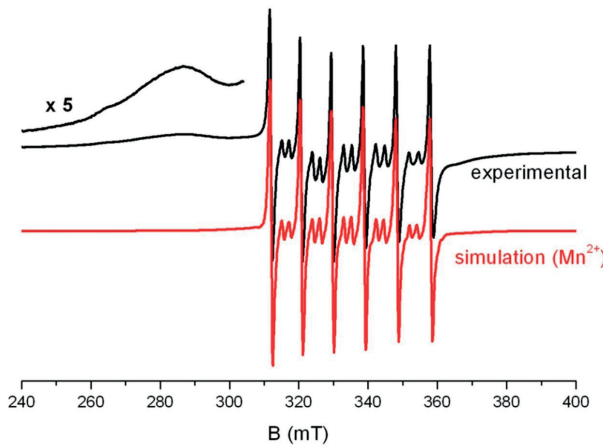

Figure 11. Experimental (black) and theoretical (red line) X-band EPR spectra from a powder sample of blue smithsonite at room temperature. EPR conditions: modulation amplitude, 1.0 Gpp; microwave power, 2.0 mW; microwave frequency, 9.38 GHz.

represents Cu^{2+} aggregations, corresponding to the Cu nanophase observed by TEM-EDS.

Conclusion

We have investigated the origin of the colour in natural blue Zn-carbonate (smithsonite) using spectroscopic and microscopic techniques. Optically, smithsonite is not homogeneous and an extensive network of blue bands is giving the bulk sample its blue colour of variable intensity. Fundamental investigation by means of XRD and laser micro-Raman spectroscopy verifies that blue smithsonite has the typical structure of the mineral and cannot reveal the cause of the blue colour. Furthermore, any ionic substitution of Zn^{2+} with other metals do not indicate any band shifting as it would be expected from the observed systematics we see when the position of the main Raman peak is plotted against the crystal ionic radii of monometallic carbonate end-members. NIR spectra also ensure that colour is not a cause of Cu-hydroxycarbonate (azurite and malachite) chromophore minerals. Point (SEM-EDS) and bulk (AAS) chemical analyses reveal the existence of noticeable amounts of Ca, Cu and Cd and small concentrations of Mg, Mn, Pb and Fe cations. This indicates that the cause

of smithsonite colouring should be searched out in the presence of copper as chromophore, because it is the only metal ion with incomplete 3d electrons of which the valence electrons can be stimulated by white light.

Transmission electron microscopy was the only method to reveal the only possible origin of smithsonite colouration. Bright-field TEM images and HR-TEM images, combined with TEM-EDS chemical analyses, revealed numerous nano-sized Cu-rich (particularly Si/Ca/Cu/As-rich) inclusions organised in bands. These inclusions do not show any topotaxial relation to smithsonite bulk. However, d-spacing values measured from the EDP patterns and corresponding TEM-EDS spectra could identify these inclusions as different phases. Irradiation instability of smithsonite under high current densities, which are usually needed for an accurate HR-TEM or TEM-EDS analysis, did not allow us to precisely identify these inclusions, which might constitute more than one mineral phase. Damage though is precluded since the effect was reduced and controllable under low electron current densities. We conclude, for the first time in the literature that the blue colour of smithsonite is caused by the above nano-phases (3-7 nm), more likely due to dispersion, scattering, interference or diffraction phenomena that these inclusions induce to the absorbed electromagnetic radiation of white light. Moreover, the replacement of Zn^{2+} by Cu^{2+} is not straightforwardly suggested by our results.

Acknowledgements

The authors want to thank the two anonimous referees and the editor Mr. Antonio Gianfagna for their contribution in the improvement of the current article. Finally, the corresponding author would like to thank the experienced amateur geologist and friend Alkiviadis Tsolakos for his in situ advices on Lavrion mines geology.

References

Abragam A. and Bleaney B. (1970) - Electron Paramagnetic Resonance of Transition Ions. (eds): Clarendon Press, Oxford.

Applin K. and Hicks B. (1987) - Fibers of dumortierite in quartz. *American Mineralogist*, 72, 170-172.

Birch W. (1986) - Zinc-manganese carbonates from Broken Hill, New South Wales. *Mineralogical Magazine*, 50, 49-53.

Böettcher M., Gehlken P., Birch W. and Usdowski E. (1993) - The rhodochrosite-smithsonite solid-solution series from Broken Hill (NSW), Australia: Geochemical and infrared spectroscopic investigations. In Neues Jahrbuch fur mineralogie monatshefte, 8, Schweizerbart Science Publishers, 352-362.

Böettcher M. (1995) - The formation of rhodochrosite-smithsonite ($MnCO_3$-$ZnCO_3$) solid-solutions at 5ºC. *Mineralogical Magazine*, 59, 481-488.

Chen T. and Chang L. (1975) - High Mg-smithsonite from Broken Hill, New South Wales, Australia. *Mineralogical Magazine*, 40, 307-308.

Frisch P., Lueth V. and Hlava P. (2002) - The colors of smithsonite: A microchemical investigation. *New Mexico Geology*, 24, 132-133.

Frost R., Hales M. and Wain D. (2007) - Raman spectroscopy of smithsonite. *Journal of Raman Spectroscopy*, 39, 108-114.

Frost R., Reddy B., Wain D. and Hales M. (2006) - An application of near infrared spectroscopy to the study of carbonate minerals - smithsonite, rhodochrosite, sphaerocobaltite and cadmium smithsonite. *Journal of Near Infrared Spectroscopy*, 14, 317-324.

Frost R., Reddy B., Hales M. and Wain D. (2008) - Near infrared spectroscopy of the smithsonite minerals. *Journal of Near Infrared Spectroscopy*, 16, 75-82.

Gaillou E., Post J., Rost D. and Butler J. (2012) - Boron in natural type IIb blue diamonds: Chemical and spectroscopic measurements. *American Mineralogist*, 97, 1-18.

Garcia-Guinea J., Crespo-Feo E., Correcher V., Rubio J., Roux M. and Townsend P. (2009) - Thermo-optical detection of defects and decarbonation in natural smithsonite. *Physics and Chemistry of Minerals*, 36, 431-438.

Goreva J., Ma C. and Rossman G. (2001) - Fibrous nanoinclusions in massive rose quartz: The origin of rose coloration. *American Mineralogist*, 86, 466-472.

Götte T., and Richter K. (2004) - Quantitative high

resolution cathodoluminescence spectroscopy of smithsonite. *Mineralogical Magazine*, 68, 199-207.

Hales M. and Frost R. (2007) - Synthesis and vibrational spectroscopic characterization of synthetic hydrozincite and smithsonite. *Polyhedron*, 26, 4955-4962.

Hitzman M., Reynolds N., Sangster D., Allen C. and Carman C. (2003) - Classification, genesis and exploration guides for nonsulfide zinc deposits. *Economic Geology*, 98, 685-714.

Hochella M., Lower S., Maurice P., Penn R., Sahai N., Sparks D. and Twining B. (2008) - Nanominerals, mineral nanoparticles, and earth systems. *Science*, 319, 1631-1635.

Katerinopoulos A., Solomos C. and Voudouris P. (2005) - Lavrion smithsonites. A mineralogical and mineral chemical study of their coloration. In: *Mineral deposit research: Meeting the global challenge*. (eds): J. Mao and J. Bierlein, Springer Verlag, 983-986.

Kibar R., Guineab J., Cetina A., Selvia S., Karalc T. and Cand N. (2007) - Luminescent, optical and color properties of natural rose quartz. *Radiation Measurements*, 42, 1610-1617.

Ma C., Goreva J. and Rossman G. (2002) - Fibrous nanoinclusions in massive rose quartz: HRTEM and AEM investigations. *American Mineralogist*, 87, 269-276.

Ma C. and Rossman, G. (2008) - Barioperovskite, $BaTiO_3$, a new mineral from the Benitoite mine, California. *American Mineralogist*, 93, 154-157.

Nassau K. (1978) - The origins of colour in minerals. *American Mineralogist*, 63, 219-229.

Plathe K., Von der Kammer F., Hassellöv M., Moore J., Murayama M., Hofmann T. and Hochella M. (2010) - Using FlFFF and a TEM to determine trace metal-nanoparticle associations in riverbed sediment. *Environmental Chemistry*, 7, 82-93.

Reddy B., Yamauchi J., Ravikumar R., Chandrasekhar A. and Venkataramanaiah M. (2004) - Optical and EPR investigations on smithsonite minerals. *Radiation Effects and Defects in Solids*, 159, 141-147.

Reeder R. (1983) - Crystal Chemistry of the Rhombohedral Carbonates. In: Reviews in Mineralogy. Carbonates: Mineralogy and Chemistry. (eds): R. Reeder, pp. 399, Mineralogical Society of America, 1-48.

Shalimova V. and Khirin N. (1969) - Model for the green photoluminescence of polycrystalline cadmium sulfide films. *Russian Physics Journal*, 12, 373-375.

Shannon R. (1976) - Revised effective ionic radii and systematic studies of the interatomic distances in halides and chalcogenides. *Acta Crystallographica*, A32, 751-767.

Skarpelis N. and Argyraki A. (2008) - Geology and origin of supergene ore at the Lavrion Pb-Ag-Zn deposit, Attika, Greece. *Resource Geology*, 59, 1-14.

Udubasa G., Constantinescu S., Popesku-Pogrion N., Hirtopanu P. and Udubasa S. (2007) - Nano-minerals identification by different physical techniques. *Romanian Reports in Physics*, 59, 819-824.

Waychunas G. (2001) - Structure, aggregation and characterization of nanoparticles. In: Nanoparticles and the environment. Reviews in Mineralogy and Geochemistry. (eds): J. Banfield and A. Navrotsky E, Mineralogical Society of America, 105-166.

Waychunas G. and Zhang H. (2008) - Structure, chemistry, and properties of mineral nanoparticles. *Elements*, 4, 381-387.

Submitted, December 2014 - Accepted, June 2015